

# Instrument Response Functions of the Antarctic Demonstrator for the Advanced Particle-astrophysics Telescope (ADAPT)

# Wenlei Chen,<sup>a,\*</sup> James H. Buckley<sup>b</sup> and Marion Sudvarg<sup>b</sup> for the APT collaboration

<sup>a</sup> Oklahoma State University,
145 Physical Sciences Bldg, Stillwater, OK, USA
<sup>b</sup> Washington University in St. Louis,

One Brookings Drive, Saint Louis, MO, USA

E-mail: wenlei.chen@okstate.edu

The Antarctic Demonstrator for the Advanced Particle-astrophysics Telescope (ADAPT) gammaray/cosmic-ray instrument serves as a precursor to the proposed APT mission. The APT mission is designed to improve sensitivity in the MeV-TeV gamma-ray range by an order of magnitude compared to current missions and is optimized for dark-matter and multimessenger research. The ADAPT instrument uses scintillating fibers for particle tracking and sodium-doped cesium iodide (CsI:Na) tiles read out with wavelength shifting (WLS) fibers for imaging, with solid-state silicon photomultipliers (SiPMs) for calorimetry. It includes four layers of imaging calorimeter detectors and scintillating-fiber trackers, functioning both as a Compton and Pair telescope for gamma-ray measurements from several hundred keV to several GeV. The ADAPT balloon flight aims to advance the technical readiness for the APT gamma-ray mission concept and, during its long duration flight, will provide better sensitivity to 1-100 MeV transients than Fermi or other gamma-ray instruments. We have optimized event reconstruction models based on simulations incorporating the optical properties of CsI tiles, WLS signal attenuation measurements, and SiPM and preamplifier board characterizations. The realistic detector construction been simulated and the instrument's response has been evaluated as functions of both the incident gamma-ray direction and gamma-ray energy. We present the Instrument Response Functions (IRFs) for APT and ADAPT, including the detectors' effective area, angular resolution as given by the point-spread function (PSF), and energy dispersion.

39th International Cosmic Ray Conference (ICRC2025) 15–24 July 2025 Geneva, Switzerland



<sup>\*</sup>Speaker

#### 1. Introduction

The Advanced Particle-astrophysics Telescope (APT) is a proposed gamma-ray and cosmic-ray observatory planned for orbit around the sun-Earth L2 point. Using a multilayer tracker and an imaging calorimeter, APT will detect gamma rays from hundreds of keV to a few TeV. Its design features 3-meter scintillating fibers with silicon photomultiplier readouts, maximizing the effective area and field of view. The detector combines scintillating fiber trackers with a calorimeter made of thin sodium-doped CsI layers and crossed wavelength-shifting (WLS) fibers for precise energy measurements. To validate the capabilities of the APT instrument and to evaluate gamma-ray and cosmic-ray reconstruction algorithms, we designed the Antarctic Demonstrator for APT (ADAPT), which is a high-altitude balloon experiment that utilizes approximately 1% of the sensitive material incorporated in the complete APT detector. The mission will offer real-time alerts and localization for gamma-ray bursts (GRBs) and other gamma-ray transients detected during the planned Antarctic flight. Detailed descriptions of the scientific goals of APT and ADAPT and instrument design can be found in [3, 4, 10]. The current status of the APT and ADAPT missions project is described in [10].

To validate instrument design, simulation code and gamma ray / cosmic ray reconstruction algorithms were developed for the APT and ADAPT detectors [4]. High-level synthesis algorithms for electronic data processing in particle astrophysics detectors have also been created, applied to the ADAPT balloon mission to process thousands of sensor channels for gamma-ray detection efficiently [11, 12]. Based on optical simulations and laboratory tests, including studies of CsI tile optical properties, WLS signal attenuation measurements, and characterizations of silicon photomultiplier (SiPM) and preamplifier boards, these front-end electronic models are now integrated into the APT and ADAPT simulations and considered in event reconstruction.

Although previous studies focused on detecting and reconstructing Compton scattering MeV events and developing the ADAPT and APT instruments to improve GRB alerts and localization [6] (see recent progress in ADAPT performance modeling and advancements in GRB source localization in [7]), the APT mission also aims to improve the effective area for GeV gammaray observations. With the updated front-end electronic models integrated into the simulation, we optimize our event reconstruction algorithms accordingly. We further analyze the instrument capabilities to detect single gamma-ray events and derive instrument response functions (IRFs) for APT and ADAPT, including the detectors' effective area, angular resolution (as described by point-spread functions, PSFs) and energy dispersion. This article presents updated IRFs based on our latest developments.

#### 2. Simulation and Reconstruction of Gamma-Ray Events

#### 2.1 Detector Simulations

Gamma-ray and cosmic-ray events for the APT and ADAPT detectors are simulated using Geant4 [1]. The APT's sensitive detector comprises 20 tracker/imaging CsI-calorimeter (ICC) layers, each with a  $3m \times 3m \times 5mm$  CsI:Na crystal and 2mm square WLS fiber planes in both x and y directions, plus cylindrical scintillating fibers arranged in two interleaved x/y planes per layer. As illustrated in Fig. 1, the ADAPT detector has 4 ICC layers and 3 additional CsI-calorimeter layers to

increase radiation length, each built from  $3 \times 3$  tiles of  $15 \text{cm} \times 15 \text{cm} \times 5 \text{mm}$  CsI:Na crystals. A 1mm tungsten sheet with 1cm thick scintillator is placed beneath the calorimeter layers for additional albedo radiation veto.

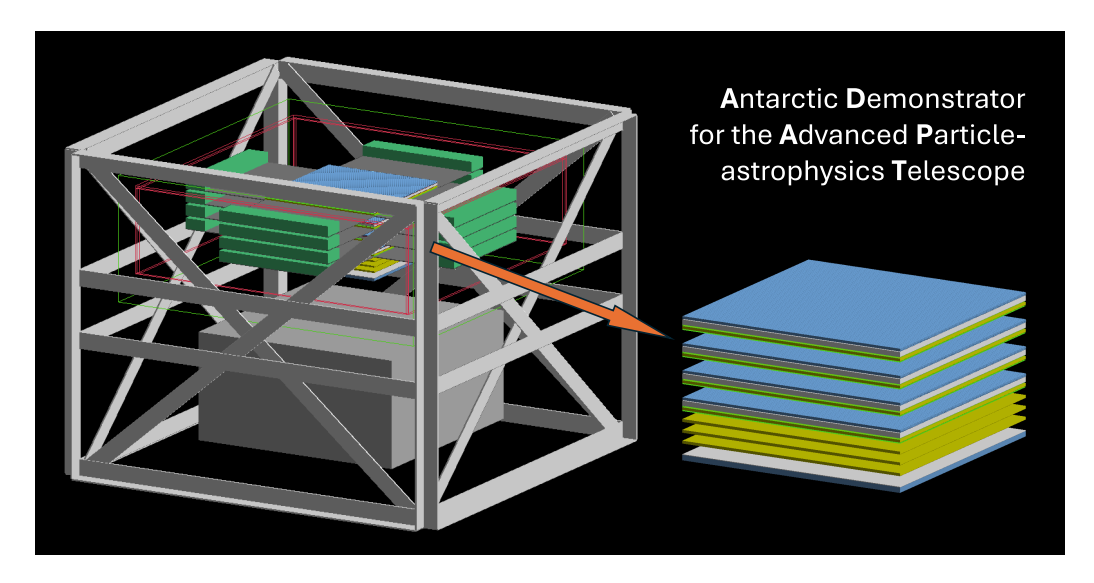


**Figure 1:** Geometry of the ADAPT payload and sensitive detector for the Geant4 [1] simulation. The ADAPT sensitive detector consists of 4 fully instrumented ICC layers and 3 additional CsI-calorimeter layers on bottom.

The balloon-borne ADAPT detector receives gamma rays, protons, electrons, neutrons, and other particles from solar system objects (including Earth's atmospheric radiations), the Milky Way, and extragalactic sources. Interactions between these particles and surrounding materials can generate additional gamma rays and secondary particles, contributing to the instrument background noise. In the ADAPT simulation, we construct a detailed mass model of the ADAPT payload (as shown in Figure 1), including the main heavy components of the balloon instruments. The mass model allows us to simulate the instrument background and optimize the event-reconstruction algorithms in the presence of these backgrounds.

# 2.2 Reconstruction of Gamma-Ray Events

The APT instrument operates as both a pair telescope for 30 MeV to  $\sim 1$  TeV  $\gamma$ -rays and a Compton telescope with sensitivity down to  $\sim 0.3$  MeV. Pair production dominates above  $\sim 0.3$  MeV, while below  $\sim 10$  MeV, gamma rays primarily undergo multiple Compton scatterings before depositing energy or escaping. Reconstruction methods for Compton and pair events differ, resulting in an energy gap at  $\sim 10-30$  MeV where neither mode is effective. As described in [4], to reconstruct pair events, a two-step algorithm first estimates the shower direction via linear regression, identifies the primary hit where the electron-positron pair is produced, and then refines the direction by assessing signals consistent with secondary peaks. Detailed Compton event reconstruction algorithms are described in [4, 6]. For energy reconstruction, we develop a simple particle shower fitting algorithm for pair events. In the lower-energy regime, we integrate optical signals from ICC fibers and edge detectors for Compton events.

Using realistic and optimized models of optical signals, measurements of energy deposition are calibrated by correcting for fiber attenuation loss and dark counts. As illustrated in Figure 2, during a gamma ray event, the optical signals collected are significantly affected by the noise of dark counts and optical contamination. To implement event-reconstruction algorithms, signal islands are identified to enable accurate measurement of the particle shower in the detector. A signal island is defined as a group of adjacent activated channels that meet a specified signal-to-noise ratio cut, have a width greater than a minimum number of fibers, and possess a total optical signal intensity exceeding a corresponding energy threshold. The two right panels in Figure 2 show how particle showers can be identified using these signal islands, as well as how the primary hit required to reconstruct the direction of the pair event can be detected.

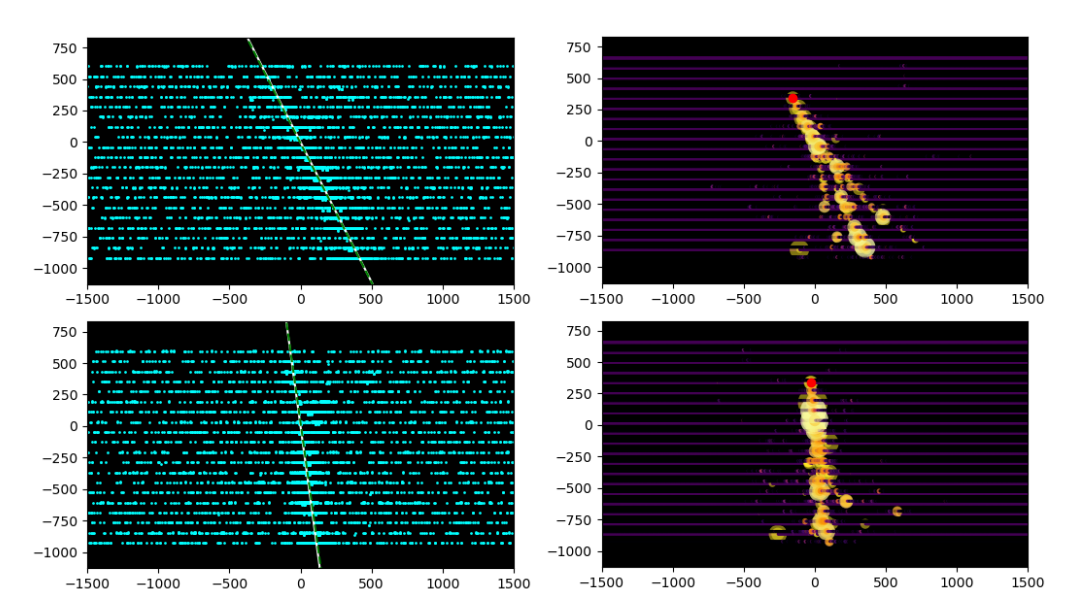


**Figure 2:** An example of a 1 GeV gamma-ray event recorded by the APT detector: The two panels on the left display the XZ-plane and YZ-plane channels that detect optical signals during the event. The two panels on the right show the corresponding signal islands identified for this event, where the size and color of each island in the figure indicate the width and intensity, respectively. The red dots marked in the right panels denote the primary hits detected in the XZ and YZ planes. The coordinates are given in mm.

#### 3. Instrument Response Functions

Instrument performance is assessed by statistically calculating the differences between parameters obtained from simulated gamma rays and those obtained from reconstructed events. The IRFs for APT and ADAPT in detecting gamma rays are characterized by three key factors: efficiency of the gamma-ray detection represented by the effective area, angular resolution measured by the PSF, and energy resolution represented by the energy dispersion.

#### 3.1 Effective Area and Geometric Factor

The effective area is a crucial aspect of the IRF that quantifies the capability of a gamma-ray telescope to detect resolvable gamma rays. The key parameters affecting detection efficiency are the

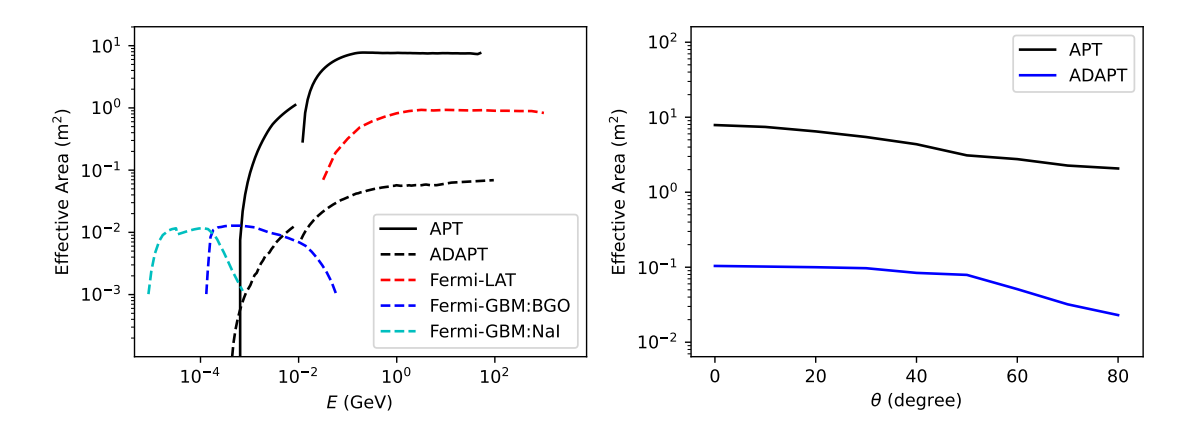


**Figure 3:** Effective area of APT and ADAPT. Left: The plot shows the normal-incident effective area as a function of gamma ray energy E. Solid black curves represent APT, while dashed black curves correspond to ADAPT. The dashed red curve indicates Fermi P8R2\_SOURCE\_V6 events, and dashed blue and cyan curves display the Fermi-GBM effective area for the BGO and NaI detectors, respectively. Right: The effective area is plotted as a function of inclination angle  $\theta$  for 1 GeV gamma rays. Black and blue curves correspond to APT and ADAPT, respectively.

angle of inclination relative to the detector's Z-axis  $(\theta)$  and the energy (E) of the incident gamma ray.

Detection efficiency is assessed across the full range of these parameters to provide comprehensive coverage for both the APT and the ADAPT instruments. In this study, we calculate the effective area for eight inclination angle bins spanning  $\theta = 0^{\circ}$  to  $\theta = 80^{\circ}$ . At  $\theta = 90^{\circ}$ , the effective area approaches zero for pair events due to the improbability that the resulting particle shower will be detected by multiple ICC layers. Gamma-ray events are simulated using a power-law spectrum  $(E^2 dN/dE \propto E^{-\beta})$  with an index  $\beta = -0.5$ , which optimizes computational efficiency and ensures adequate sample sizes within each logarithmic energy interval. For each inclination angle bin, 10<sup>6</sup> gamma rays are generated over the energy range of 0.3 MeV to 1 TeV. The azimuthal angle  $\phi$  is also randomized, and the events are correspondingly binned. However, given the limited size of the

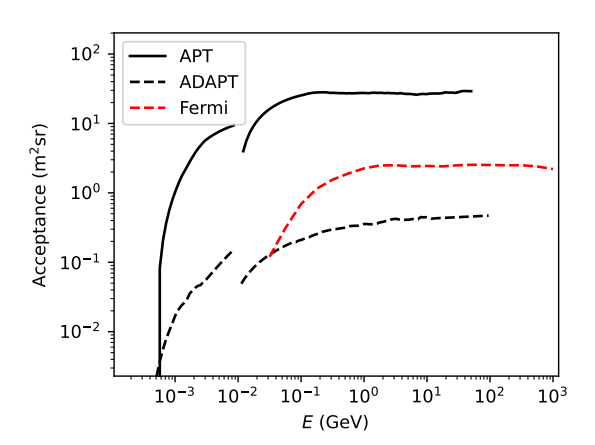


**Figure 4:** Geometric factor of APT and ADAPT: The plot shows the geometric factor as a function of gamma ray energy *E*. Solid black curves and dashed black curves represent APT and ADAPT respectively, while the dashed red curve indicates Fermi P8R2\_SOURCE\_V6 events.

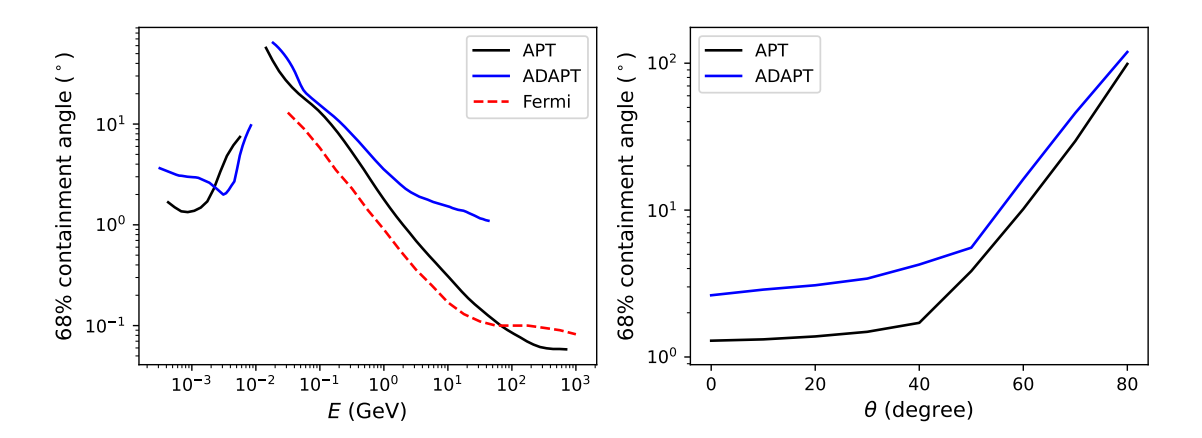
current simulation dataset, the observed dependence of  $\phi$  in the effective area is negligible relative to the statistical fluctuations inherent in Monte Carlo sampling. Furthermore, it should be noted that the dependence of phi has a minimal impact on the analyses that integrate over long time intervals.

Figure 3 shows that APT achieves an effective area approximately one order of magnitude larger than Fermi-LAT [2], with values in the MeV range reaching  $\sim 0.1-1 \text{m}^2$ , significantly surpassing previous Compton telescopes such as COMPTEL [9]. The effective area of ADAPT is roughly two orders of magnitude smaller than that of the full APT detector, which is consistent with its reduced geometric size. In the  $\gtrsim 1$  MeV energy regime, the effective area of ADAPT is comparable to that of the Fermi-GBM detectors. The geometric factor is defined as the effective area integrated over the solid angle, as shown in Figure 4.

### 3.2 Point Spread Functions (PSFs)

The PSFs for APT and ADAPT are determined by the angular offset  $\Delta\theta$  between the reconstructed and true gamma-ray directions. The PSFs depend on the energy of the incoming photon (E) and the inclination angle  $(\theta)$ , but do not vary significantly with the azimuthal angle  $\phi$ . For Compton events,  $\Delta\theta$  is defined as the minimum offset from the true direction of the event to the reconstructed Compton ring for each event. Note that this  $\Delta\theta$  differs from the GRB localization error described in [4, 5, 7], which uses numerous reconstructed rings.

Similarly to Fermi-LAT PSFs [2], the distribution of angular offset between the reconstructed and true gamma-ray directions can be described by the Moffat function [8]. For each specific E and  $\theta$ , the function parameters are fitted to the reconstruction results to generate the PSFs for APT and ADAPT. As shown in Figure 6, the count density in each bin of  $\Delta\theta^2$  is accurately reproduced using the analytical PSF based on the Moffat function. The results indicate that APT provides an angular resolution comparable to Fermi Pass 8 SOURCE events, particularly at energies above 10 GeV.



**Figure 5:** Angular resolution of APT and ADAPT. Left: The plot shows the acceptance-weighted 68% containment angle of  $\Delta\theta$  as a function of gamma ray energy E. Solid black and blue curves represent APT and ADAPT, respectively, while the dashed red curve indicates Fermi P8R2\_SOURCE\_V6 events. Right: The 68% containment angle is plotted as a function of inclination angle  $\theta$  for 1 GeV gamma rays. Black and blue curves correspond to APT and ADAPT, respectively.

#### 3.3 Energy Dispersion

The energy dispersion is measured as the fractional difference between the reconstructed (E') and the true energy (E). We evaluated  $\Delta E/E$  (where  $\Delta E=|E-E'|$ ) based on the gamma-ray

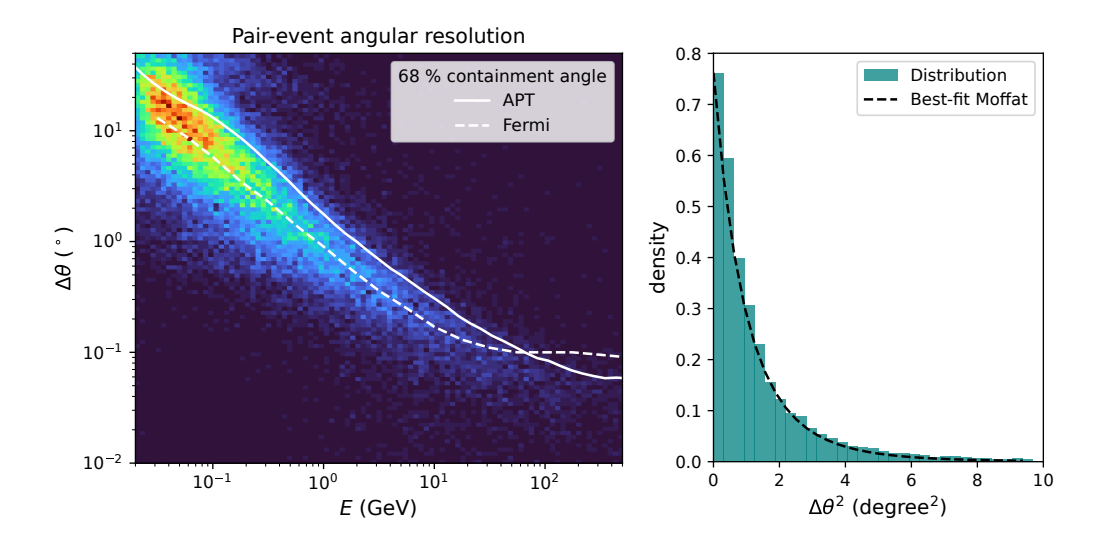


**Figure 6:** Left: Distribution of  $\Delta\theta$  as a function of E for APT. Solid and dashed curves show the 68% containment of APT and Fermi-LAT P8R2\_SOURCE\_V6 events, respectively. Right: Distribution of count rate in each uniform  $\Delta\theta^2$  bin as a function of  $\Delta\theta^2$  for APT at 1 GeV. The dashed curve shows the best-fit Moffat function to this distribution.

energy (E) and the angle of inclination  $(\theta)$ . To achieve a large area but limited by the payload capacity of the launch vehicles, the APT calorimeter, with 5.4 CsI radiation lengths (approximately 5.8 including fibers and supports), is significantly shallower than the Fermi-LAT  $\sim 10$  radiation lengths. As shown in Figure 7, APT achieves a dispersion of energy < 40% throughout its detection range and performs better than 20% for energies  $\lesssim 1-4$  MeV and  $\sim 0.1-1$  GeV. ADPAT offers comparable results to APT in the Compton regime, but has poor resolution at above 1 GeV due to its limited radiation lengths.

## 4. Discussion

Using multiple layers of a scintillating fiber tracker and a distributed ICC with a combined thickness of less than 6 radiation lengths, APT prioritizes a large detection area and rapid all-sky coverage over energy resolution. The imaging calorimeter enables the instrument to operate both as a pair telescope and a Compton telescope, providing sensitivity across energies from 0.3 MeV to 1 TeV. The effective area of the APT instrument extends to several square meters, exceeding that of previous experiments. Although angular and energy resolution in the Compton regime may be limited, the instrument's large effective area and high detection efficiency are expected to enhance the gamma-ray sensitivity of MeV substantially.

ADAPT has been constructed to test the APT design. Improvements have been made to event reconstruction algorithms using updated front-end models for signal collection and the mass model of the ADAPT payload. This mass model facilitates the reconstruction of gamma-ray events while accounting for instrumental background. It should be noted that atmospheric gamma rays generated by cosmic-ray interactions are classified as signals rather than the instrument background in this analysis (see detailed models described in [5]). The simulation incorporates the optical

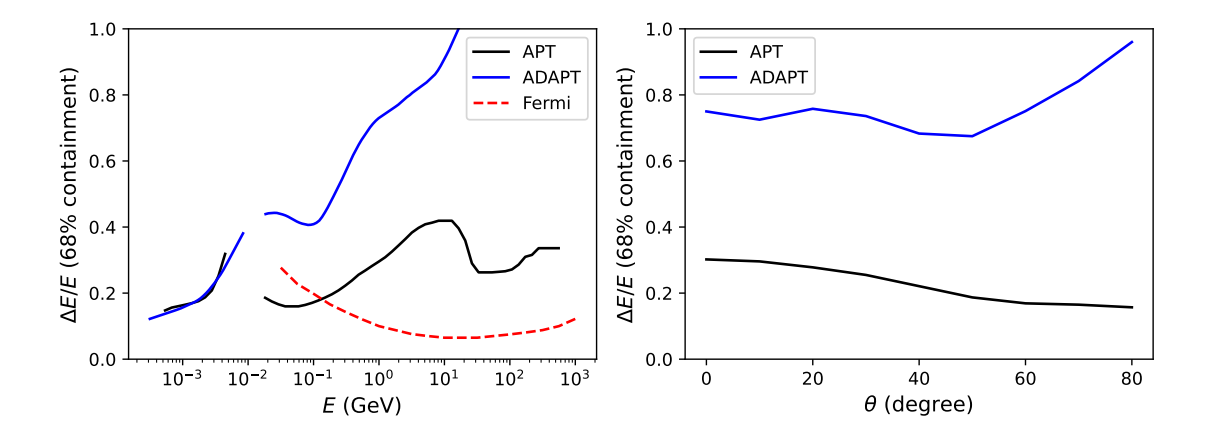


**Figure 7:** Energy resolution of APT and ADAPT. Left: The plot shows the acceptance-weighted 68% containment of  $\Delta E/E$  as a function of gamma ray energy E. Solid black and blue curves represent APT and ADAPT, respectively, while the dashed red curve indicates Fermi P8R2\_SOURCE\_V6 events. Right: The 68% containment of  $\Delta E/E$  is plotted as a function of inclination angle  $\theta$  for 1 GeV gamma rays. Black and blue curves correspond to APT and ADAPT, respectively.

properties of CsI tiles, WLS signal attenuation measurements, and SiPM and preamplifier board characterizations, indicating that APAPT can function as both a Compton and a pair telescope for the suborbital mission. Currently, IRFs are determined based on all reconstructed events, which display diversity in their energy deposition patterns within the detectors. Further classification of these reconstructed event types is expected to allow the selection of gamma-ray events with improved angular and energy resolution. Each event class and type selection will have specific IRFs, which will be determined in future analyses.

#### References

- [1] Agostinelli, S., Allison, J., Amako, K., et al. 2003, Nuclear Instruments and Methods in Physics Research A, 506, 250
- [2] Ajello, M., Atwood, W. B., Axelsson, M., et al. 2021, The Astrophysical Journal Supplement Series, 256, 12
- [3] Buckley, J., Nussirat, S. A., Altomare, C., et al. 2021, in ICRC 2021, Astroparticle Physics Conf.
- [4] Chen, W., & Buckley, J. 2021, in ICRC 2021, on behalf of the APT Collaboration
- [5] Chen, W., & Buckley, J. 2023, in ICRC 2023, on behalf of the APT Collaboration
- [6] Htet, Y. 2023, in ICRC 2023, on behalf of the APT Collaboration
- [7] Htet, Y., Sudvarg, M., Buhler, J., et al. 2025, in ICRC 2025, on behalf of the APT Collaboration
- [8] Moffat, A. F. J. 1969, Astronomy and Astrophysics, 3, 455
- [9] Schoenfelder, V., Aarts, H., Bennett, K., et al. 1993, Astrophysical Journal Supplement, 86, 657
- [10] Serini, D., & Venere, L. D. 2025, in ICRC 2025, on behalf of the APT Collaboration
- [11] Sudvarg, M. 2023, in ICRC 2023, on behalf of the APT Collaboration
- [12] Sudvarg, M., Chamberlain, R., & Buckley, J. 2025, in ICRC 2025, on behalf of the APT Collaboration

#### **Acknowledgments**

This work was supported by NASA award 80NSSC21K1741.